Korean J. Chem. Eng., 34(11), 2886-2900 (2017)
DOI: 10.1007/s11814-017-0216-9

pISSN: 0256-1115
eISSN: 1975-7220

Preparation and characterization of a novel nanocomposite of clinoptilolite/maghemite/chitosan/urea for manganese removal from aqueous solution

Zahra Sareban and Vahid Javanbakht†

ACECR Institute of Higher Education (Isfahan Branch), Isfahan, 84175-443, Iran
(*Received 15 May 2017 • accepted 4 August 2017*)

Abstract−Synthesis of a new magnetic nanocomposite of Clinoptilolite/Maghemite/Chitosan/Urea has been carried out to introduce an adsorbent to remove manganese as a toxic heavy metal from aqueous solution. Clinoptilolite zeolite became magnetic using the maghemite nanoparticles, then coated using chitosan as a biodegradable and non-toxic polymer, and finally functionalized by urea to increase the adsorption capacity. For characterization of the nanocomposite, the X-Ray diffraction, IR spectroscopy, vibrating sample magnetometery, and scanning electron microscopy were used. The effects of temperature, contact time, initial metal concentration, solution pH and adsorbent dose on the manganese removal capacity were evaluated. The kinetics of adsorption by the pseudo-first-order, pseudo-second-order, and Elovich kinetic models was studied and the results suggested the compliance of pseudo-second-order kinetic model with the kinetic data. The maximum adsorption capacity of manganese under the optimum condition of pH=2.13, the adsorbent amount of 0.02 g, initial solution concentration of 46.00 mg/L with response surface methodology, equaled 16.30 mg/g. The Langmuir, Freundlich, Temkin and Dobinin-Rudoshkovich adsorption isotherm models were investigated and Langmuir best fit the isotherm data. In the study of the thermodynamic results, negative Gibbs free energy represents the spontaneous nature of manganese removal process.

Keywords: Manganese, Nanocomposite, Adsorption, Maghemite, Clinoptilolite

INTRODUCTION

One of the most important global issues is environmental pollution caused by hazardous toxic heavy metals [1,2]. Heavy metal toxicity is due to the strong urge of cations to disrupt the activity of essential enzymes in living organisms [3,4]. Among toxic pollutants, manganese is a metallic element found in the earth's crust which can lead to economic and health problems [5-8]. Potassium permanganate is an inorganic chemical compound and medication and is very toxic to aquatic organisms. Potassium permanganate solutions of about 1 percent can harm the gastrointestinal system and could be fatal. Higher concentrations of potassium permanganate, about 2 percent to 3 percent, can cause anemia and swelling of the throat leading to suffocation. In an acidic solution, permanganate is reduced to the +2 oxidation state of the manganese (II) ion. Manganese with a density ranging from 7.21 to 7.44 g·cm^{-3} is considered a heavy metal and is one of the pollutants of surface and underground water sources, poisoning with which results in acute effects on the nervous system and blood system. Considering the above-mentioned drawbacks, removing manganese compounds such as potassium permanganate from aqueous solutions is very important and necessary [9,10]. Removal of heavy metals from aqueous solutions is considered to be an important issue in public health. Already, several methods have been developed for removing heavy metals like manganese from solutions such as adorption, ion exchange, reverse osmosis, ultrafiltration, chemical precipitation, and oxidation [11-13]. Among these, adsorption is an effective and acceptable way for heavy metal removal [1,5,14]. Zeolites are primarily composed of aluminosilicate ions with high cation exchange capacity, high specific surface area and mesh-like structure [15]. Clinoptilolite is the most common natural zeolite which belongs to heulandite family with a chemical formula of $KNa_2Ca_2(Al_7Si_{29})O_{72}\cdot 24H_2O$. Natural and synthetic zeolites with high adsorption capacity can be used for polluted waters treatment. Clinoptilolite, an abundant and cheap zeolite used in the preparation of fertilizers, concrete and pollutants adsorbents, can be easily obtained from mines [16,17]. Although the separation of clinoptilolite powder from large volumes of the suspension is usually difficult, magnetic adsorbents simply solve this problem [18]. Magnetizing adsorbents to facilitate their separation from adsorbent suspension is of practical interest. Maghemite nanoparticle is one of the magnetic nanoparticles used to produce composite adsorbent for wastewater treatment [19]. High specific surface area, the high prevalence of active sites and high magnetic property of magnetic nanoparticles increase the adsorption efficiency and pollutant removal rate and make it easy to separate adsorbent from solution through a magnetic field [20]. Several well-known methods including co-precipitation [21], reverse micelles [22], thermal, and hydrothermal synthesis [23] are used in the synthesis of magnetic nanoparticles. Co-precipitation is a simple technique for maghemite synthesis [23]. Chitosan as a non-toxic, biocompatible, biodegradable and available natural polymer and its derivatives are used as adsorbents for removing heavy metals. To improve the mechanical properties, adsorption capacity, and prevent the adsorbent dissolution in acidic solutions, chitosan with different crosslinkers such as glutaraldehyde has been used [24].

†To whom correspondence should be addressed.
E-mail: v.javanbakht@ce.iut.ac.ir

We synthesized Clinoptilolite/Maghemite/Chitosan/Urea magnetic nanocomposite and then used it for manganese removal. Clinoptilolite was magnetized using maghemite magnetic nanoparticles, coated by chitosan and then functionalized by urea to increase the adsorption capacity. The synthesized magnetic nanocomposite was characterized by VSM, XRD, SEM, FTIR analyses. The effects of the temperature, contact time, metal concentration, pH, and the adsorbent dosage on the manganese removal capacity were investigated. The adsorption kinetics, isotherms and thermodynamics studies were performed. Response surface methodology and central composite design were used to achieve optimal conditions in manganese removal and for experimental design.

EXPERIMENTAL PROCEDURE

1. Material

All solutions were prepared using deionized water and all materials were used in analytical grade. Powdered clinoptilolite with the chemical formula of $KNa_2Ca_2(Al_7Si_{29})O_{72}\cdot 24H_2O$ and average particle size of 1 micron collected from central Alborz mountain range located in Iran.

2. Preparation of Clinoptilolite/Maghemite Nanocomposite

Before synthesizing nanocomposite, zeolite particles were processed and pretreated. 5 g clinoptilolite was put in 5 M HCl solution for 24 h. The treated product was then rinsed with distilled water thrice to reach neutral pH and dried in an oven at room temperature. Maghemite nanoparticles (γ-Fe_2O_3) were synthesized by a single-stage method under quasi-neutral conditions without the need for oxidation and organic solvents [25,26]. For nanocomposite synthesis (with different weight ratios of maghemite/clinoptilolite: 1 : 1, 1 : 2 and 1 : 3), a special amount of treated clinoptilolite was added to water and placed on the stirrer for 10 minutes at room temperature to reach the clinoptilolite distribution. $FeCl_3\cdot 6H_2O$ and $FeCl_2\cdot 4H_2O$ with a molar ratio of 1 : 2 at 293, 323 and 353 K were added to a very dilute aqueous HCl solution and were put on the stirrer for 10 min to get iron salts dissolved completely. Then the salts solution and zeolite suspension were mixed together. Furthermore, 2 M NaOH solution was added dropwise to the mixture for 90 min under inert conditions. At the beginning, the solution was milky but after NaOH addition, a brown precipitate formed which got darker as time passed. Finally, the precipitate was separated from the suspension by a magnet, then rinsed once by ethanol and thrice by distilled water and was dried in an oven at 80 °C for 8 hr.

3. Preparation of Clinoptilolite/Maghemite/Chitosan/Urea Nanocomposite

A certain amount of nanocomposite (with maintaining the weight ratio of 5 : 1 for nanocomposite/chitosan) was distributed in water and was stirred for 10 min at room temperature. A few drops of glutaraldehyde solution 25% was added to the suspension as a crosslinker. A solution of chitosan dissolved in 1% acetic acid solution was prepared and added dropwise to the previous suspension of nanocomposite (maghemite/zeolite/chitosan) for 30 min, and it

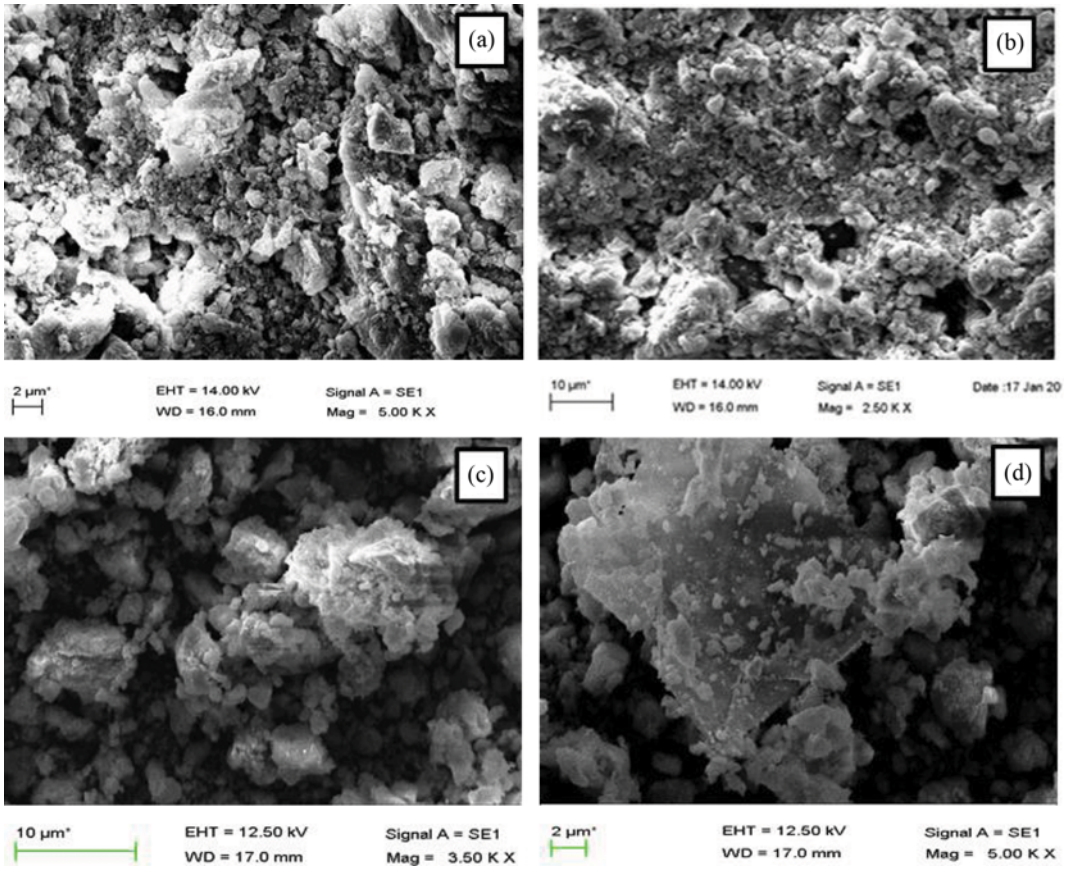

Fig. 1. SEM images of ((a) and (b)) Clinoptilolite, ((c) and (d)) Clinoptilolite/Maghemite/Chitosan/Urea nanocomposite.

took 30 more minutes for coating to be completed. Then, the precipitate was separated from the suspension by a magnet and rinsed three times with distilled water and dried in an oven at 70 °C. To increase the adsorption capacity, urea, which is composed of two amino groups and one carbonyl functional group, was added to nanocomposite. For this purpose, nanocomposite was dispersed in water on the stirrer for 10 min. Then some urea (with 1 : 1 weight ratio of urea/chitosan) was dissolved in water and stirred at 60 °C at 300 rpm for 1 hr, and then was added drop by drop to the nanocomposite suspension for 30 min. Then, the precipitate was separated from the suspension by a magnet and rinsed three times with distilled water and dried in an oven at 60 °C. Finally, nanocomposite (Clinoptilolite/Maghemite/Chitosan/Urea) was obtained.

4. Characterization

Crystal and phase structures of nanocomposite were specified using an irradiation of Cu Kα (λ=0.154 nm) in the range of 10-80° (2θ) with JEOL JDX-8030 diffractometer (X-Ray Diffraction (XRD)). Using XRD method, nanometer particles sizes can be determined by Scherrer equation under specific circumstances. The size and morphology of the synthesized particles were assessed by scanning electron microscopy (SEM, Zeiss EVO 50electron). To determine the type of synthesized samples and the functional groups in their structure and to ensure the successfulness of nanocomposite coating, the Fourier transform infrared spectrometer Jasco-4200 (FTIR) was used. The saturation magnetization and magnetic properties of nanocomposite were assessed under various conditions using a vibrating sample magnetometer (VSM, MPMS-5 SQUID). The solution concentration was determined by a Rayleigh-UV-2601 spectrophotometer.

5. Removal Study

A solution of manganese ions was prepared by dissolving potassium permanganate in distilled water at concentrations of 10-50 mg/*l* of permanganate. To adjust pH on 2-6, 0.1 M NaOH and 0.1 M HCl solutions were used. Generally, a certain amount of magnetic nanocomposite (0.01-0.05 g) was well dispersed in 25 ml of permanganate solution. Nanocomposite and permanganate mixture was stirred in a shaker at 200 rpm. Then, the magnetic adsorbent was separated from the solution by a magnet and its adsorption capacity was measured using UV-spectrophotometer. The adsorption capacity can be calculated using the following equation:

$$q_t = \frac{(C_0 - C_t) \times V}{M} \quad (1)$$

$$q_t = \frac{(C_0 - C_e) \times V}{M} \quad (2)$$

where q_t, C_0, C_t, C_e, V and M are adsorption capacity (mg/g), initial concentrations (mg/*l*), concentration at time t (mg/*l*), equilibrium concentration (after adsorption) (mg/*l*), solution volume (ml), and amount of adsorbent (g), respectively.

RESULTS AND DISCUSSION

1. Characterization

1-1. SEM Analysis

The size and morphology of the Clinoptilolite/Maghemite/Chitosan/Urea nanocomposite were examined by scanning electron microscope (Fig. 1). Figs. 1(a) and (b) show the SEM images of clinoptilolite. According to these images, there are many pores on the surface of clinoptilolite. As can be seen in Figs. 1(c) and (d), maghemite magnetic nanoparticles are found on the clinoptilolite surface, and the structure of zeolite and maghemite was not changed by chitosan coating.

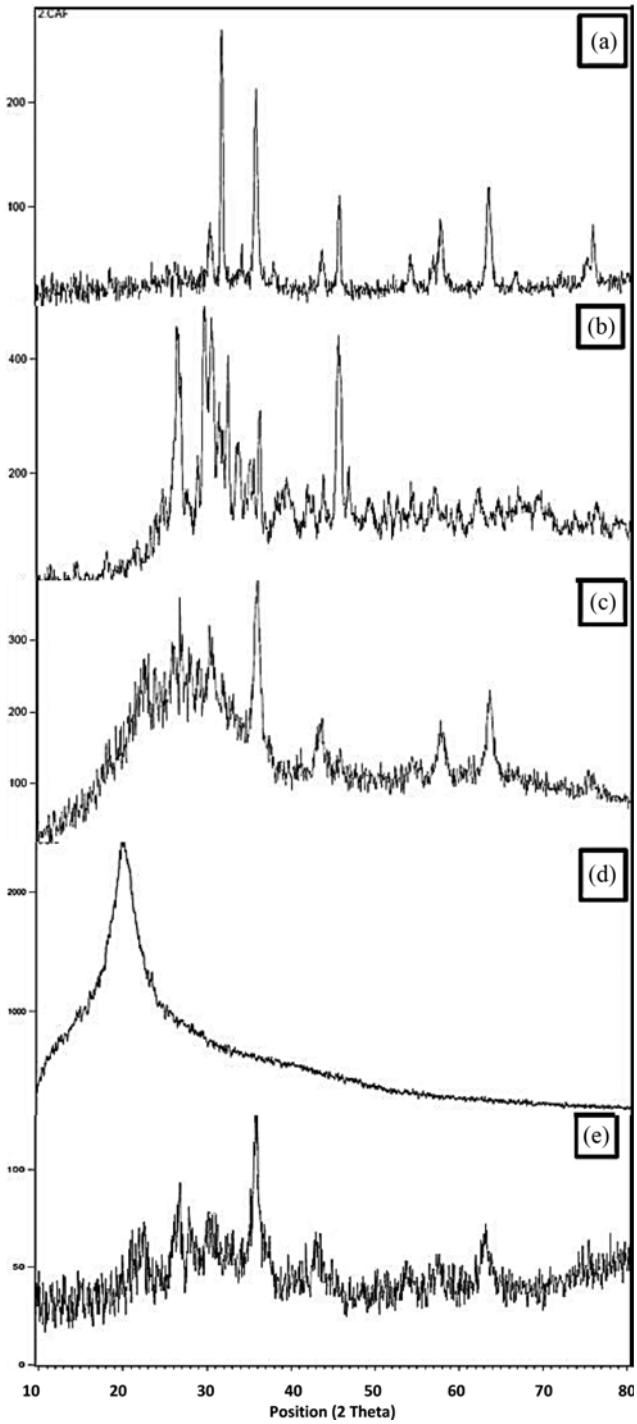

Fig. 2. XRD results of (a) Maghemite (b) Clinoptilolite, (c) clinoptilolite/Maghemite nanocomposite, (d) Chitosan, (e) Clinoptilolite/Maghemite/Chitosan//Urea nanocomposite.

1-2. XRD Results

Fig. 2 shows the X-ray diffraction results for maghemite nanoparticles, clinoptilolite, clinoptilolite/maghemite/chitosan nanocomposite and maghemite/clinoptilolite/chitosan/urea nanocomposite. It can be observed that the peaks belonging to all pure components of the nanocomposite have not changed, which indicates that nanocomposite components have retained their original structure during the composition. The X-ray diffraction results of maghemite/clinoptilolite/chitosan/urea nanocomposite reveal that peaks at 2θ=30.3, 35.9, 43.1, 57.7, and 63.2° are represented by (2 2 0), (3 1 1), (4 0 0), (5 1 1), (4 4 0) phases. Moreover, Fig. 2(e) shows the chitosan peak and zeolite peaks at 2θ=20.2° and 2θ=22.3, 26.7, 27.1, and 43.3° respectively. Using Eq. (3), the Scherrer formula and based on X-ray diffraction data, the average particle size was calculated as about 14 nm.

$$\tau = \frac{K\lambda}{\beta\cos\theta} \tag{3}$$

where τ, K, λ, β, and θ are the average size of nanoparticles (nm), crystal shape factor (0.9), the wavelength of the X-ray tube (nm), peak's full width at half maximum height, and the diffraction angle, respectively.

1-3. VSM Results

One of the main characteristics of this nanocomposite is its magnetic properties, which were determined using VSM. Fig. 3 shows the curve of the magnetic properties (saturation magnetization) of maghemite nanoparticles, clinoptilolite, Clinoptilolite/Maghemite and Clinoptilolite/Maghemite/Chitosan/Urea nanocomposite at 298 K. As applied external magnetic field intensity increases, the magnetization increases until saturation magnetization is reached. As can be seen, the curve is S-shaped, which is indicative of superparamagnetic properties of the nanocomposite. Magnetizing clinoptilolite facilitates the clinoptilolite separation from adsorbent suspension and pollutant-containing solution, and is considered an advantage of the synthesized nanocomposite. Once the external magnetic field is removed, nanocomposite will be quickly dispersed by shaking. Based on Fig. 3, the saturation magnetization of maghemite nanoparticles and zeolite adsorbent was 50.09 and 0 emu g^{-1}, respectively. Following zeolite/maghemite nanocomposite synthesis and precipitation of maghemite nanoparticles on the base of clinoptilolite adsorbent the saturation magnetization reduced to 22.93 emu g^{-1}. Coating and functionalization of clinoptilolite/maghemite nanocomposite led to the reduction of its magnetic properties. Nanocomposite saturation magnetization decreased from 22.93 to 18.43 emu g^{-1} as it was coated with chitosan and functionalized with urea for surface modification. The decrease observed in the saturation magnetization of nanoparticles is due to lower weight percentage of maghemite in them. From Fig. 4 that displays the saturation magnetization curves of clinoptilolite/maghemite nanocomposites synthesized with different weight ratios of maghemite/clinoptilolite of 1 : 1, 1 : 2 and 1 : 3, it can be concluded that nanocomposite saturation magnetization decreases as clinoptilolite amount increases. From the saturation magnetization curve of clinoptilolite/maghemite nanocomposite synthesized at 20, 50 and 80 °C which is showed in Fig. 5, the saturation magnetization of nanocomposite increases with synthesis temperature. It can be partly explained, on one hand, by the fact that oxygen dissolution decreases by increasing the temperature and thus surface oxidation of particles is reduced. And on the other hand, crystallization improvement with temperature results in the formation of more maghemite phase and increases magnetic property accordingly. As temperature increases, both the magnetic and the crystallite sizes increase. A major reason for this is the thickness of the nonmagnetic layer deposited on the surface of particles, which is known as a dead layer. This layer is the result of surface oxidation, non-crystallization and non-alignment of the electron spins and

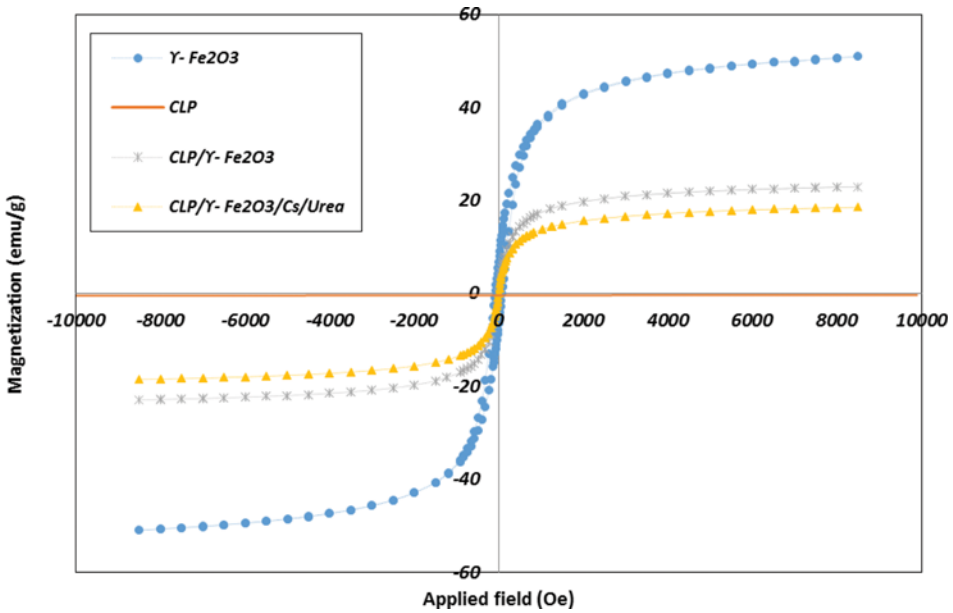

Fig. 3. VSM results of Maghemite, Clinoptilolite, Clinoptilolite/Maghemite nanocomposite, and Clinoptilolite/Maghemite/Chitosan/Urea nanocomposite.

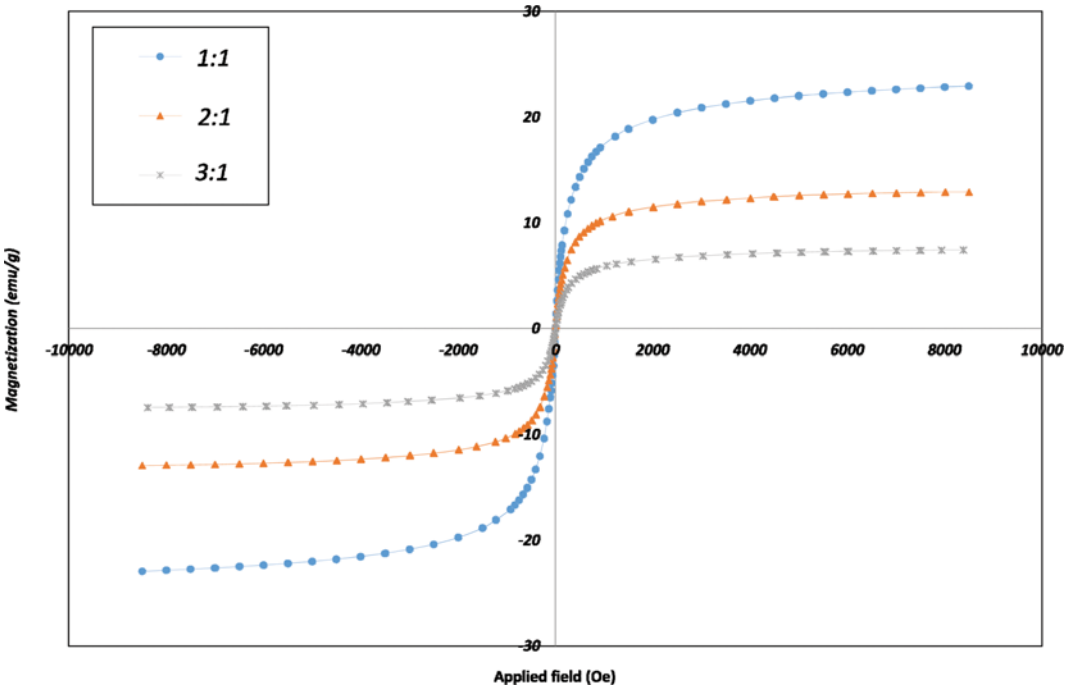

Fig. 4. VSM results of Clinoptilolite/Maghemite nanocomposite with different weight ratio of Clinoptilolite/Maghemite.

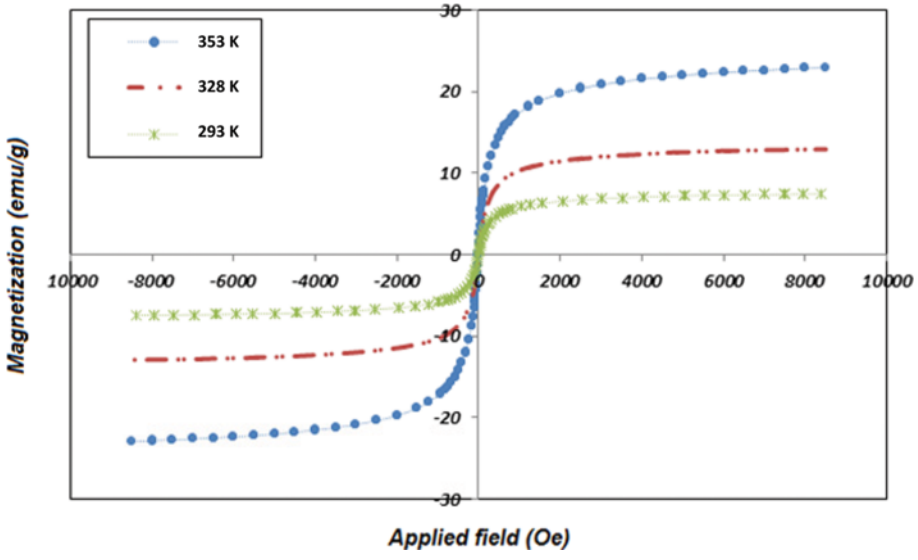

Fig. 5. VSM results of Clinoptilolite/Maghemite nanocomposite in different temperature of synthesis (293, 323, and 353 K).

has no magnetic property.

1-4. FTIR Results

Clinoptilolite FTIR spectrum is depicted in Fig. 6(a). This spectrum shows that the absorption visible at 3,420 cm^{-1} is related to terminal chemical groups of the outer surface of clinoptilolite crystal structure [18,27]. This peak overlaps broad and strong peaks related to O-H stretching bond centered at 3,420 cm^{-1} [28]. The peak at 1,641 cm^{-1} is associated with O-H bending vibrations. The peak at 797 cm^{-1} is a result of stretching and bending bonds of Si-O and Al-O in clinoptilolite structure. The peak observed at 1,090 cm^{-1} indicates both symmetric and asymmetric stretching bonds inside the tetrahedron [18,27]. From the maghemite spectrum shown in Fig. 6(b), the peak around 3,396 cm^{-1} could be associated with stretching mode of H_2O molecules or hydroxyl groups on the surface of maghemite nanoparticles. The peak around 1,617 cm^{-1} is also linked to bending vibrations of H_2O. The peak at 579 cm^{-1} which belongs to iron-oxygen bond shows interstitial stretching vibrations of iron in tetrahedral sites [29]. Whereas, iron-oxygen bond at 424 cm^{-1} is related to octagonal stretching bond of iron [18]. Chitosan spectrum (Fig. 6(d)) represents a strong peak at 3,432 cm^{-1} which are associated with stretching vibrations of O-H, extensive vibrations of N-H and polysaccharide internal hydro-

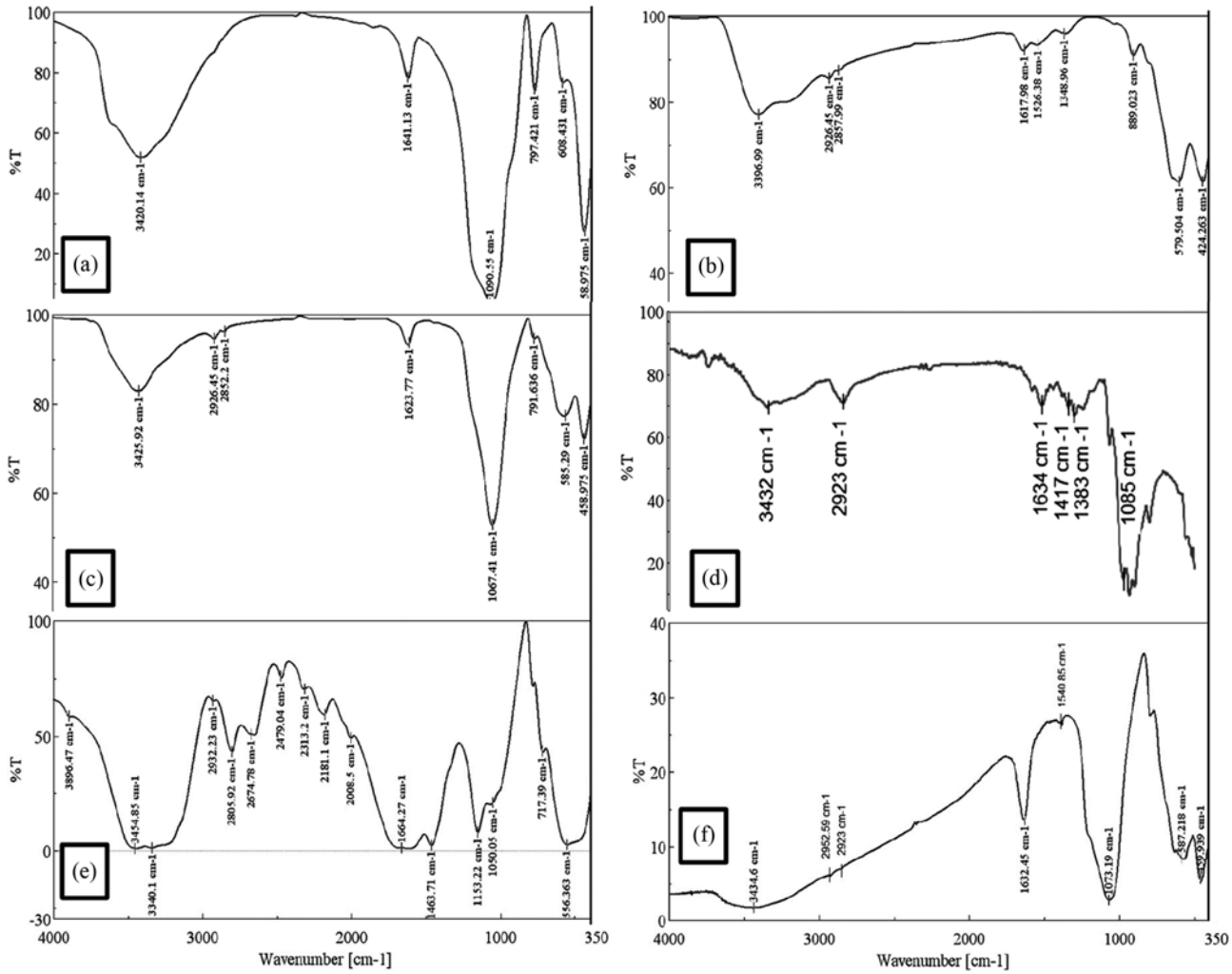

Fig. 6. FTIR results of (a) Clinoptilolite, (b) Maghemite, (c) Maghemite/Clinoptilolite nanocomposite, (d) Chitosan, (e) Urea, (f) Maghemite/Clinoptilolite/Chitosan/Urea nanocomposite.

gen bonds. The peak visible at 2,923 cm^{-1} shows C-H stretching vibrations [18,30], while the peak centered at 1,634 cm^{-1} may be attributed to the stretching vibrations of NHCO, C=O along with bending bonds of N-H and NH_2 [31]. The adsorption peaks at 1,417, 1,383, 1,085 cm^{-1} may be related to stretching vibration of C-N, bending vibration of CH_3 and stretching vibration of C-OH. The peaks centered at 2,932, 1,664, 1,463, 1,153 cm^{-1} in urea spectrum (Fig. 6(e)) are apparently related to stretching bonds of N-H, C-H, C=C, C-O, and C-N, respectively. In addition, absorption peaks in the range 3,000-3,896 cm^{-1} are associated with O-H stretching vibration which overlaps N-H-related peaks. In Clinoptilolite/Maghemite/Chitosan/Urea nanocomposite spectrum (Fig. 6(f)), in addition to the absorption characteristic of chitosan functional groups bonds, there is a peak at 587 cm^{-1} which is caused by Fe-O, showing that the chitosan can successfully cover maghemite nanoparticles in clinoptilolite/maghemite nanocomposite through electrostatic interactions. Absorption peaks centered at 2,952, 1,540 and 3,434 cm^{-1} (corresponding to N-H and O-H bonds) suggest that urea has managed to overlay the surface of clinoptilolite/maghemite/chitosan nanocomposite [18,30].

2. Adsorption Studies

2-1. Adsorption Kinetics

The adsorption kinetics indicates the correlation between physical and chemical characteristics of the adsorbate particles, adsorbent, and the influence of adsorption mechanism. To investigate the mechanism of the adsorption processes, such as the chemical reaction, mass transfer, and diffusion-controlled reaction, several kinetic models were used in different experimental conditions [24]. In this study, the kinetic models including the pseudo-first-order, pseudo-second-order intraparticle diffusion and Elovich models were studied. The pseudo-first-order kinetic model can be written as:

$$\log(q_e - q_t) = \log q_e - k_1 \times t \quad (4)$$

where, k_1 is the rate constant of pseudo-first-order adsorption (min^{-1}). The linear form of the pseudo-second-order kinetic model can be expressed as follows:

$$\frac{t}{q_t} = \frac{1}{k_2 q_e^2} + \frac{t}{q_e} \quad (5)$$

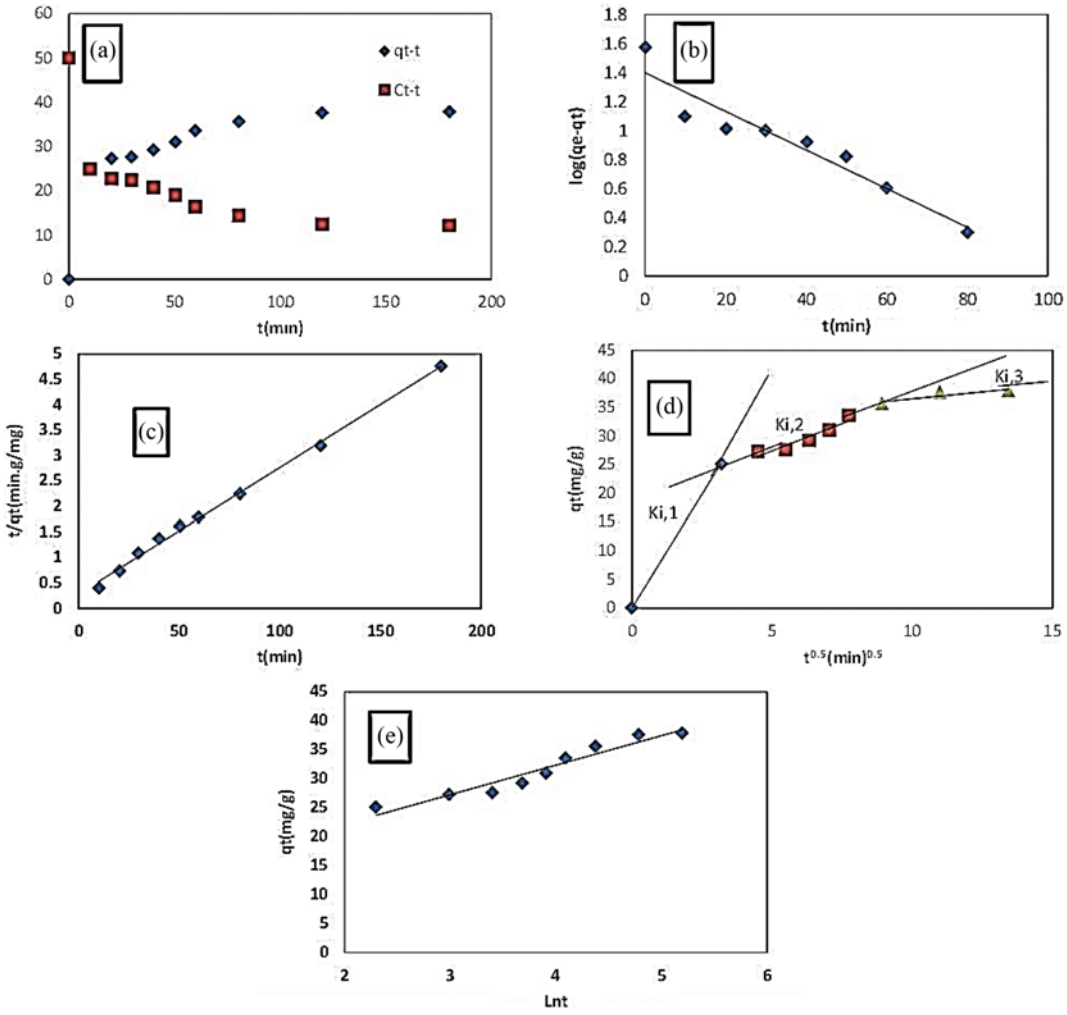

Fig. 7. Plots of (a) Kinetic data of the adsorption process, (b) Pseudo-first-order, (c) pseudo-second-order, (d) intraparticle diffusion, and (e) Elovich kinetic models of the adsorption process (for a 50 mg/L permanganate solution at pH=3).

$$h = k_2 q_e^2 \quad (6)$$

where k_2 is the rate constant of pseudo-second-order adsorption (min^{-1}), and h is the adsorption rate. The pseudo-first-order and pseudo-second-order models consist of penetration in the external film, intraparticle diffusion, and interaction between adsorbate ions and adsorbent's functional groups. The intraparticle diffusion is a transitional process, which describes the motion of particles from the solution to the solid phase. The intraparticle diffusion model is described by the following equation:

$$q_t = k_i t^{0.5} + C \quad (7)$$

where, k_i and C are the intraparticle diffusion rate constant, and the particle diffusion rate constant of the boundary layer, respectively. Elovich model used to the interpret chemical kinetics is defined as:

$$q_t = \frac{1}{\beta}\ln(\alpha\beta) + \frac{1}{\beta}\ln t \quad (8)$$

where, α is the initial adsorption/desorption rate constant, and β is the activation energy of the adsorbent.

Fig. 7(a) shows the concentration decay versus time. The permanganate adsorption in different concentrations was investigated. As can be seen, nearly 50% of the adsorption is accomplished within the first 10 minutes. The percentage and capacity of adsorption increase as time passes. This increase in adsorption capacity continues until the system reaches equilibrium and the adsorbent becomes saturated. From this figure, it can be found that the adsorbent reaches equilibrium at the first 120 minutes and shows a nearly constant trend after that. Evaluating permanganate adsorption kinetic models according to the correlation coefficient (R^2) reveals that the adsorption process complies more with the pseudo-second-order kinetic model. The pseudo-second-order model involves penetration in the external film, intraparticle diffusion, and interaction between adsorbate ions and adsorbent functional groups. This model suggests that permanganate is adsorbed quickly and chemical adsorption process is rate-controlling [32]. Fig. 7(d) shows that the permanganate adsorption is carried out in more than just one diffusion step. $K_{i,1} > K_{i,2} > K_{i,3}$ indicates three different steps of the permanganate adsorption at the outer surface, the inner sur-

face, and equilibrium, respectively [18,32].

2-2. Adsorption Isotherm

In adsorption, an equilibrium is established between solutes adsorbed on the adsorbent surface and solutes in the solution. The concentration of solute adsorbed on the adsorbent surface plotted against the concentration of solute in the solution at equilibrium at a given temperature expresses the adsorption isotherm, which can be described by different models. Parameters related to these models provide important information about the adsorbent internal bonds, adsorption mechanism, and surface properties [18]. The experimental data were fitted with several different models. Freundlich isotherm model, which has been used to characterize heterogeneous adsorption systems, is defined as:

$$\ln q_e = \ln k_f + \frac{1}{n}\ln C_e \tag{9}$$

where k_f is the Freundlich constant for maximum adsorption capacity, and n is the heterogeneous factor. Langmuir model which has been successfully applied to a large number of monolayer adsorption processes. One of its basic assumptions is that the adsorption occurs at particular homogeneous sites of the adsorbent. This model can be expressed as follows:

$$\frac{C_e}{q_e} = \frac{1}{k_L q_{max}} + \frac{C_e}{q_{max}} \tag{10}$$

in which q_{max} and k_L are the maximum adsorption capacity (mg/g) and Langmuir adsorption constant, respectively. R_L, the dimensionless parameter that determines the type of adsorption process, is expressed by the following equation:

$$R_L = \frac{1}{1 + k_L C_0} \tag{11}$$

Adsorption could be desirable ($0<R_L<1$), undesirable ($R_L>1$), linear ($R_L=1$), or irreversible ($R_L=0$) [16,30]. Dubinin-Radushkevich model, which is used to differentiate between chemical and physical adsorption, is in the form of:

$$\ln q_e = \ln q_m - B\varepsilon^2 \tag{12}$$

where q_m and β are the maximum capacity to adsorb ions and a constant related to adsorption average energy, and ε is given by the following equation:

Table 1. Kinetic parameters of different kinetic models

Kinetic model	Kinetic parameters	
Pesudo-first order	K_1 (1/min)	0.0133
	q_e (exp.) (mg/g)	25.10152
	R^2	0.9116
Pesudo-second order	K_2 (g/(mg·min)	0.002179
	q_e (mg/g)	40.322
	h (mg/(g·min)	3.542
	R^2	0.997
Elovich	α (mg/g min^{-1})	53.025
	β (g/mg)	0.196044
	R^2	0.9313
Intraparticle diffusion	$K_{i,1}$ (mg/(g/$min^{0.5}$)	7.9344
	$K_{i,2}$ (mg/(g/$min^{0.5}$)	1.9131
	$K_{i,3}$ (mg/(g/$min^{0.5}$)	0.4856

$$\varepsilon = RT\ln\left(1 + \frac{1}{C_e}\right) \tag{13}$$

R is the universal gas constant (8.314 J/mol·k) and T is temperature. Free energy of transferring one mole of the solution to the adsorbent surface, that is average energy E, is given by:

$$E = \frac{1}{\sqrt{2\beta}} \tag{14}$$

Temkin isotherm is based on the assumption that adsorption temperature decreases linearly rather than logarithmically as adsorbent surface coating increases. This model can be calculated as follows:

$$q_e = \frac{RT}{b_T}\ln(AT) + \frac{RT}{b_T}\ln C_e \tag{15}$$

where b_T is a constant related to sorption heat and A is a constant related to adsorption potential [18]. After evaluating Freundlich, Langmuir, Temkin and Dubinin-Radushkevich isotherm models and based on the data presented in Table 2, once R^2 correlation coefficients are compared, it can be concluded that the Langmuir model accords more with experimental data than the other models. Langmuir model postulates a monolayer adsorption (adsorbed layer does not exceed one molecule in thickness.). Adsorption only occurs in a limited certain number of identical, equivalent adja-

Table 2. Isotherm parameters of different isotherm models

T (°C)	Freundlich			Langmuir			
	n	K_F (mg/g)	R^2	q_{max} (mg/g)	K_L (L/mg)	R^2	R_l
25	5.46	6.46	0.9691	12.72	0.48	0.9984	0.03-0.17
40	3.57	9.07	0.8941	22.88	0.47	0.9990	0.04-0.17
55	2.47	9.20	0.8814	33.44	0.28	0.9933	0.06-0.25
	Temkin			Dubinin-Radashkevich			
	b_T (J/mol)	A (L/g)	R^2	β (mol^2/Kj^2)	q_{max}	R^2	
25	1401.97	0.098	0.9748	6.00E-07	11.53	0.9042	
40	650.66	0.028	0.9504	4.00E-07	19.89	0.9714	
55	388.84	0.009	0.9622	5.00E-07	26.44	0.9765	

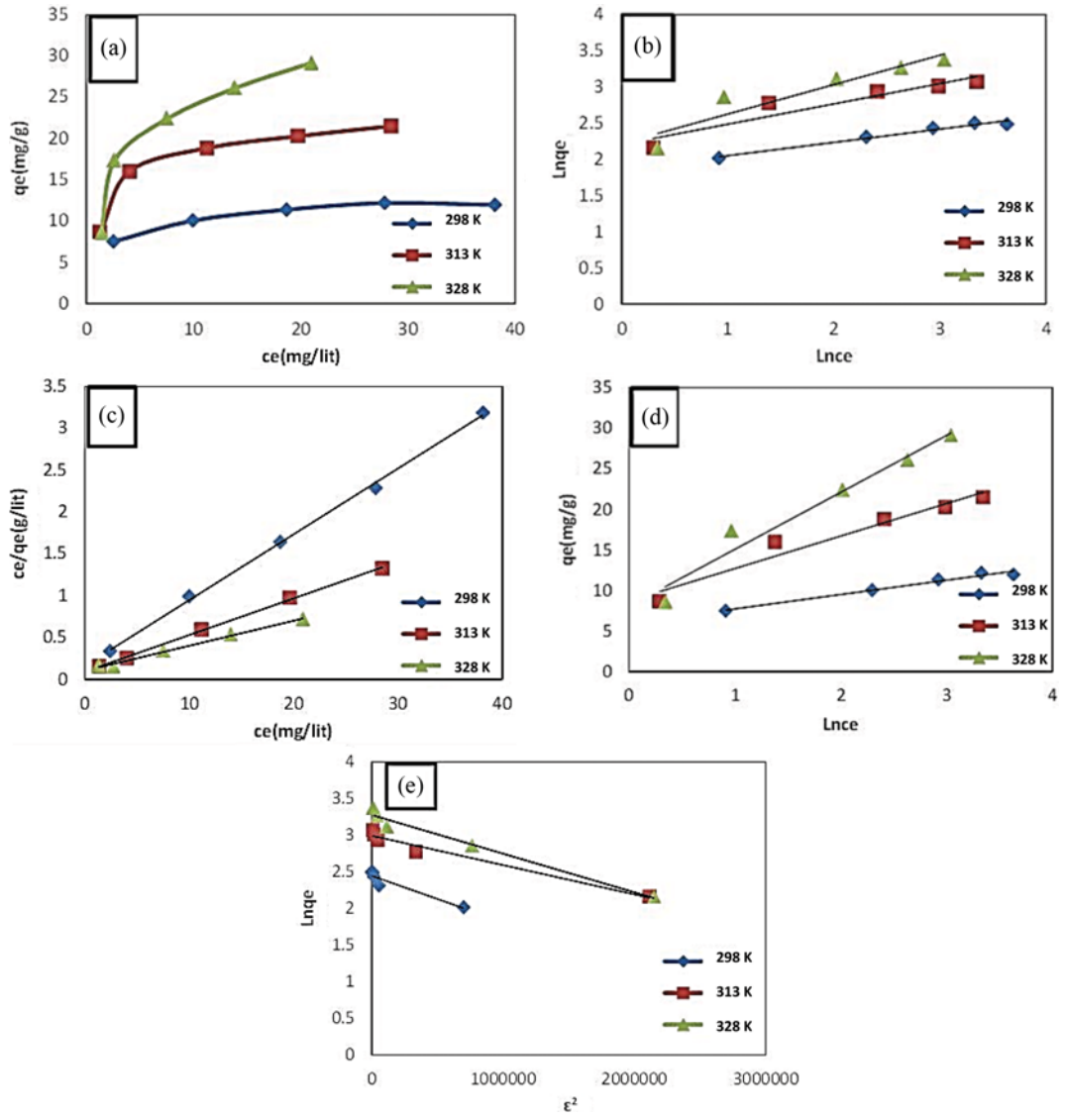

Fig. 8. Plots of (a) Isotherm data of the adsorption process in different temperature (298, 313 and 328 K), (b) Freundlich, (c) Langmuir, (d) Temkin, and (e) Dubinin-Radushkevich isotherm models (for permanganate solution with initial concentrations of 10, 20, 30, 40, 50 mg/L).

cent sites. In fact, the adsorption is restricted to a single coating layer and all sites of the surface are identical and only one atom can be adsorbed on the surface [18,33,34].

According to this model and Table 2, the maximum adsorption capacity is obtained to be 33.44 (mg/g) at 323 K. R_L varies from 0.257 to 0.395, which indicates that permanganate adsorption by nanocomposite is optimal. Also, as is evident from Fig. 8(a), which shows the effect of temperature on the permanganate adsorption capacity, adsorption capacity increases with increasing temperature. This may be due to activation of the adsorbent surface [35].

The adsorption capacities of clinoptilolite and Clinoptilolite/Maghemite/Chitosan/Urea nanocomposite for permangenate removal were determined in same conditions (3.75 and 18.54 mg/g for clinoptilolite and nanocomposite, respectively). It can be observed that the adsorption capacity increases significantly as clinoptilolite is modified by maghemite magnetic nanoparticles, covered with chitosan and functionalized by urea.

2-3. Adsorption Thermodynamics

Determination of thermodynamic parameters is another particularly important measure to describe the adsorption process. The thermodynamic parameters such as enthalpy changes, entropy changes, and Gibbs free energy changes are determined by the following equations and Lnk_d plot against 1/T (Van't Hoff plot):

$$\ln K_d = -\frac{\Delta H}{RT} + \frac{\Delta S}{R} \tag{16}$$

$$\Delta G = -RT\ln K_d \tag{17}$$

$$E_a = \Delta H + RT \tag{18}$$

R is the universal gas constant and K_d is the equilibrium constant at different temperatures [36]. In Fig. 9 Lnk_d is plotted against 1/T

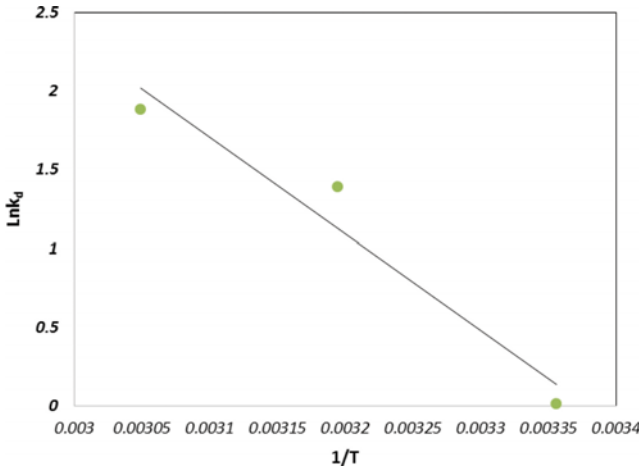

Fig. 9. The thermodynamic plot of the adsorption process (for a 20 mg/L permanganate solution at T=298, 313, 328 K).

at 298, 313 and 328 K. The K_d values were calculated with respect to Langmuir constants and the adsorption isotherm as $K_d=1/K_L=3.468$ and $K_d=q_e/C_e=6.566$, respectively [37]. Values of enthalpy, entropy, and the activation energy can be determined based on van't Hoff equation by the slope and intercept of Lnk_d versus 1/T graph. The thermodynamic parameters values were calculated using equilibrium data in Table 3. The Gibbs free energy is negative, indicating spontaneous adsorption. The positive enthalpy indicates that the interaction between the adsorbent and the pollutant is endothermic, so an increase in temperature leads to a better adsorption. This finding was confirmed by isotherm results. The positive values of entropy represent an increase of random encounters between adsorbent/solution phases during the adsorption process [18,28,36]. Also, the activation energy less than 42 kJ/mol means that the rate-controlling mechanism is diffusion [38].

Table 3. Thermodynamic parameters of the adsorption process

T (K)	E_a (KJ/mol)	ΔH (KJ/mol)	ΔS (J/mol·k)	ΔG (KJ/mol)
298	54.325			−0.027
313	54.450	51.847	172.332	−3.607
328	54.574			−4.937

3. Experimental Design

Optimization of heavy metals removal by classic method of changing an independent variable, which is kept at a constant level, is very time-consuming and costly for a large number of variables. Using experimental design and response surface methodology for heavy metals removal optimization can solve this problem. In this study, Clinoptilolite/Maghemite/Chitosan/Urea nanocomposite was used to remove permanganate. Response surface methodology was used to achieve the optimum condition of permanganate adsorption and experimental design was realized using central composite design and Design Expert software. In this design, three variables of pH, adsorbent amount, and pollutant concentration were considered. Seventeen experiments were designed with different values of pH, adsorbent amount, and pollutant concentration. To carry out these experiments, containers were prepared according to the values of the mentioned parameters and then were placed in a shaker for 120 min (the time required to reach equilibrium achieved in adsorption kinetic tests). The concentration of each sample was measured using a UV spectrophotometer at the maximum wavelength of 525 nm. The parameters and their experiment levels were determined as pH (2, 4, and 6), amount of adsorbent (0.01, 0.03, and 0.05 g), and permanganate concentration (10, 30, and 50 mg/*l*).

Findings show that there is a negligible difference between the adsorption capacity calculated by software and adsorption capacity determined in designed experiments. R^2 values in the table are also indicative of this negligible difference. Once the experimental design (Tables 4 and 5) was accomplished and the results were ob-

Table 4. The data of design of experiments

Run	A : pH	B : x	C : C	Actual value	Predicted value	Residual
1	4.00	0.03	30.00	19.5163	21.03	−1.52
2	4.00	0.03	30.00	23.4615	21.03	2.43
3	6.00	0.01	30.00	14.8252	16.48	−1.65
4	4.00	0.03	30.00	21.7483	21.03	0.72
5	2.00	0.03	10.00	8.31002	10.76	−2.45
6	6.00	0.03	10.00	7.42424	6.35	1.07
7	2.00	0.01	30.00	42.8497	40.97	1.88
8	4.00	0.01	10.00	19.4231	18.84	0.58
9	4.00	0.03	30.00	18.6655	21.03	−2.37
10	2.00	0.03	50.00	31.4161	32.49	−1.07
11	2.00	0.05	30.00	14.1818	12.53	1.65
12	6.00	0.03	50.00	15.0991	12.65	2.45
13	4.00	0.05	10.00	4.55245	3.75	0.80
14	4.00	0.05	50.00	16.2028	16.78	−0.58
15	6.00	0.05	30.00	10.9021	12.78	−1.88
16	4.00	0.03	30.00	21.7657	21.03	0.73
17	4.00	0.01	50.00	33.0245	33.83	−0.80

Table 5. The ANOVA of the permaganate adsorption on the nanocomposite

Source	Sum of squares	df	Mean square	F-value	P-value	
Model	1497.94	9	166.44	26.70	0.0001	Significant
pH	294.12	1	294.12	47.19	0.0002	
X	516.54	1	516.54	82.87	<0.0001	
C	392.46	1	392.46	62.97	<0.0001	
pH*x	153.08	1	153.08	24.56	0.0016	
pH*C	59.53	1	59.53	9.55	0.0176	
X*C	0.95	1	0.95	0.15	0.7076	
pH^2	9.99	1	9.99	1.60	0.2461	
x^2	6.05	1	6.05	0.97	0.3575	
C^2	65.00	1	65.00	10.43	0.0145	
Residual	43.63	7	6.23			
Lake of fit	28.78	3	9.59	2.58	0.1908	Not significant
Pure error	14.85	4	3.71			
Cor total	1541.58	16				

tained, the response surfaces of the optimized model were determined using regression to explain the behavior of independent variables and each response in the adsorption process. In the first step, the results of analysis of variance (ANOVA) were analyzed.

Considering data presented in Table 5, which are obtained from the ANOVA, it can be seen that the P-value of fitted model is less than 0.0001 which means that the predicted model is valid. Higher values of F and lower values of P express the importance of the desired parameter [39]. Regarding the values in the table, the first order parameters of pH, adsorbent amount, and initial concentration of permangenate, second-order parameters of adsorbent amountand initial concentration, the interactions between pH and adsorbent amountas well as pH and initial concentration are determining parameters in the process of the permangenate removal. Thus, by disregarding the less important parameters we have the following quadratic equation:

$$R_1=28.29-1.70\times pH-1163.55\times x+1.36\times C+154.65\times pH\times x-0.09\times pH\times C+2995.70\times x^2-0.01\times C^2 \quad (19)$$

The coefficient of determination or R^2 equals to 0.9717. The closer R^2 is to 1 the more important is the model and the better are the responses we get. Adjusted coefficient of determination (R^2_{adj}) states how well and how accurate the model fits experimental data. As seen in the table, the values of R^2 (0.9717) and R^2_{adj} (0.9353) are quite close to each other. The proximity of these two mentioned parameters indicates the great importance and high accuracy of the model. Another parameter is the signal to noise ratio, which has a major role in the determination of suitability of the model. Values greater than 4 are ideal for this parameter. Signal to noise value equals to 19.44 showing changes by variables in responses is appropriate and reasonable. The coefficient of variation (C.V.=13.12) indicates the reliability of experiments.

3-1. Response Surface Plots

In this section, the effect of process parameters on the adsorption capacity as well as permanganate removal as a function of pH, permanganate initial concentration, and the adsorbent amount is investigated according to Fig. 10. The removal rate of permanganate is shown as a function of pH and adsorbent amount in Fig. 10(a). As seen, permanganate removal decreases with adsorbent amount increasing from 0.01 to 0.05 g. It is also evident that permanganate removal is not ideal at pH greater than 2. Therefore, maximum adsorption capacity was achieved once pH and adsorbent amount were reduced simultaneously. Fig. 10(b) demonstrates the effect of pH and initial concentration on permanganate removal solution. For the above-mentioned reasons, permanganate removal increases with initial concentration increasing from 10 to 50 mg/*l* and pH decreasing from 6 to 2. In Fig. 10(c) permanganate removal is depicted as a function of the adsorbent amount and initial concentration of the solution (permanganate). From this figure, one can find that permanganate removal capacity increases with a decrease in adsorbent amount from 0.05 to 0.01 and an increase in adsorbate initial concentration (permanganate) from 10 to 50 mg/*l*.

By increasing the adsorbent amount, removal rate increases (Figs. 10(a), (c)), but the adsorbed permanganate per gram of adsorbent (adsorption capacity) decreases. The increased adsorbent amount could increase specific surface area and adsorption sites of adsorbent. This decline can be due to the large amounts of adsorbent or low amounts of permanganate ions compared to available adsorption sites or accumulation of large amounts of adsorbent through which permanganate ions could be repulsed by interacting particles [18,36,40,41].

The solution pH plays an important role in the adsorption process (Figs. 10(a), (b)), and in particular in adsorption capacity through modification of nanocomposite surface. pH of the solution influences the adsorption sites of adsorbent surface and permanganate chemical state [24]. At low pH, the capacity of permanganate removal could increase as a result of increment of the number of accessible sites. In fact, at low pH, the number of H^+ ions increases and negative ligands on the surface are adsorbed by them. So negative charge on the surface is reduced and its charge becomes positive. Therefore, it can remove negative ions of pollutant. In addition, at low pH hydrated ions (H_3O^+) are formed, which leads to a competition between positive charges to remove nega-

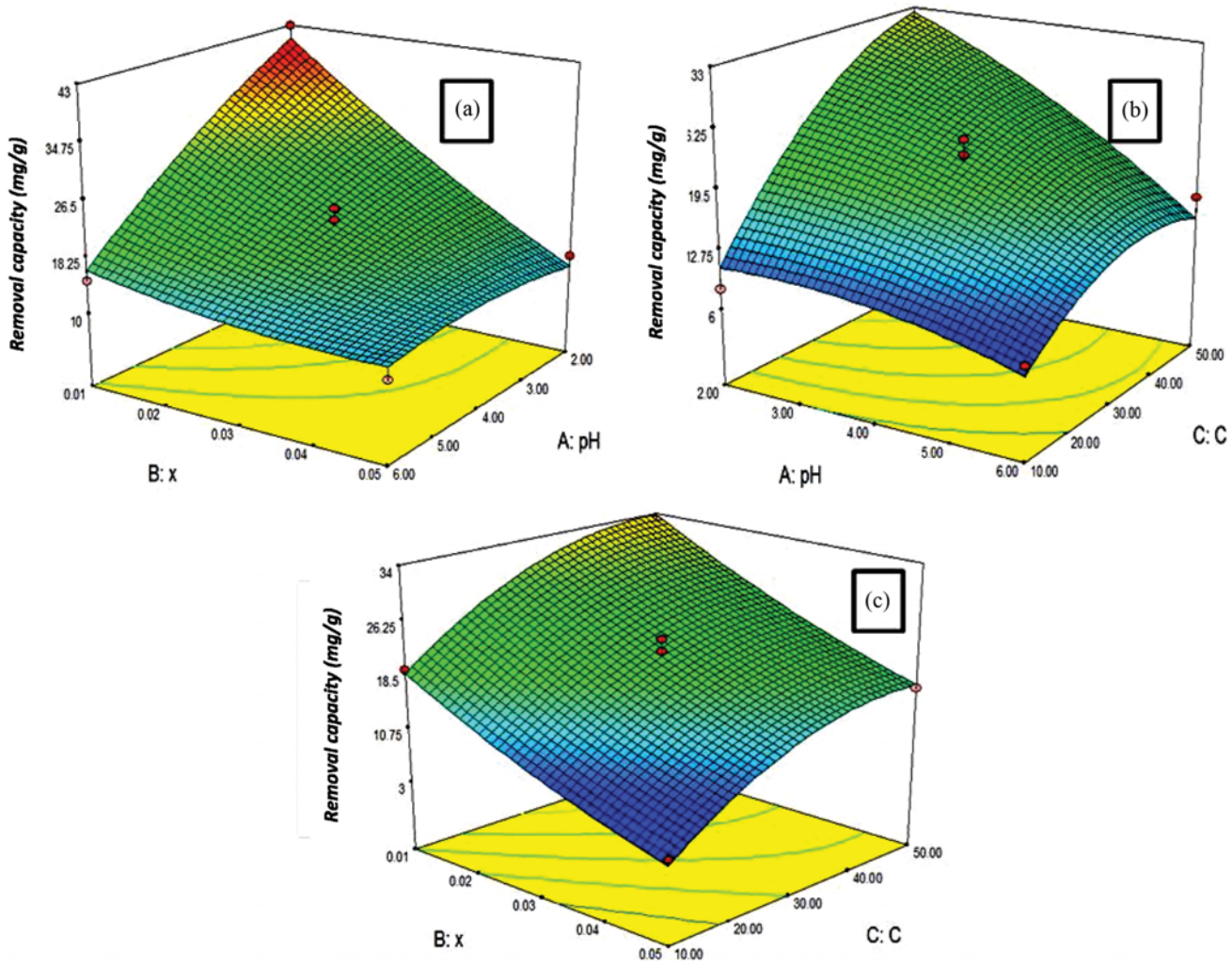

Fig. 10. Response surface plots for the effect of (a) the pH and the adsorbent amount (g) (pH=2-6 and adsorbent amounts=0.01-0.05 (g)), (b) the pH and the initial concentration (mg/L) (pH=2-6 and initial concentrations=10-50 (mg/L)); (c) and the initial concentration (mg/L) and the adsorbent amount (g) (initial concentrations=10-50 (mg/L) and adsorbent amounts=0.01-0.05 (g)), on the permanganate removal capacity.

tive ions and since the interaction between negative ions and positive charges on the adsorbent surface increases, negative ions are better removed. Functional groups of adsorbent surface like amines and hydroxyl groups of chitosan and urea amine groups are responsible for the removal of permanganate ions. In general, adsorption capacity is governed by the adsorbent surface properties [40,42].

In the wake of increasing initial concentration of adsorbate (Fig. 10(b), (c)), driving force increases due to the concentration gradient, and thereby more permanganate is removed [40,41]. At first, permanganate removal capacity increases with initial concentration. In fact, permanganate ions are able to bind to adsorption sites and increase the adsorbency of adsorbent. At higher concentrations of adsorbed ions (permanganate), adsorption sites are occupied and permanganate removal rate is reduced [18].

3-2. Analysis of Statistical Charts

Statistical charts are analyzed through Fig. 11. As shown in Fig. 11(a), residual values around the regression line are not properly distributed and are extensively dispersed. So, the resulting model is a suitable model. In Fig. 11(b) residual values are plotted against predicted response for permanganate removal. In these charts, the points should have a random distribution. It is evident that the points are randomly distributed and do not follow any specific pattern. Fig. 11(c) shows residual values versus permanganate removal based on observations order. In this chart, standardized residual values should be distributed and scattered randomly around the central line, which according to Fig. 11(c) their distribution is random. Fig. 11(d) demonstrates actual values of response against predicted values of response. This chart can predict values that the model is not able to determine. In Fig. 11(d), points are uniformly distributed around the regression line.

3-3. Removal Optimization

In numerical optimization, each parameter and its corresponding response are studied. Optimization is about finding the best setup for the process to determine the value of each affecting factor, so that one or more output parameters are optimized. Maximum removal capacity and optimal conditions for a variable are deter-

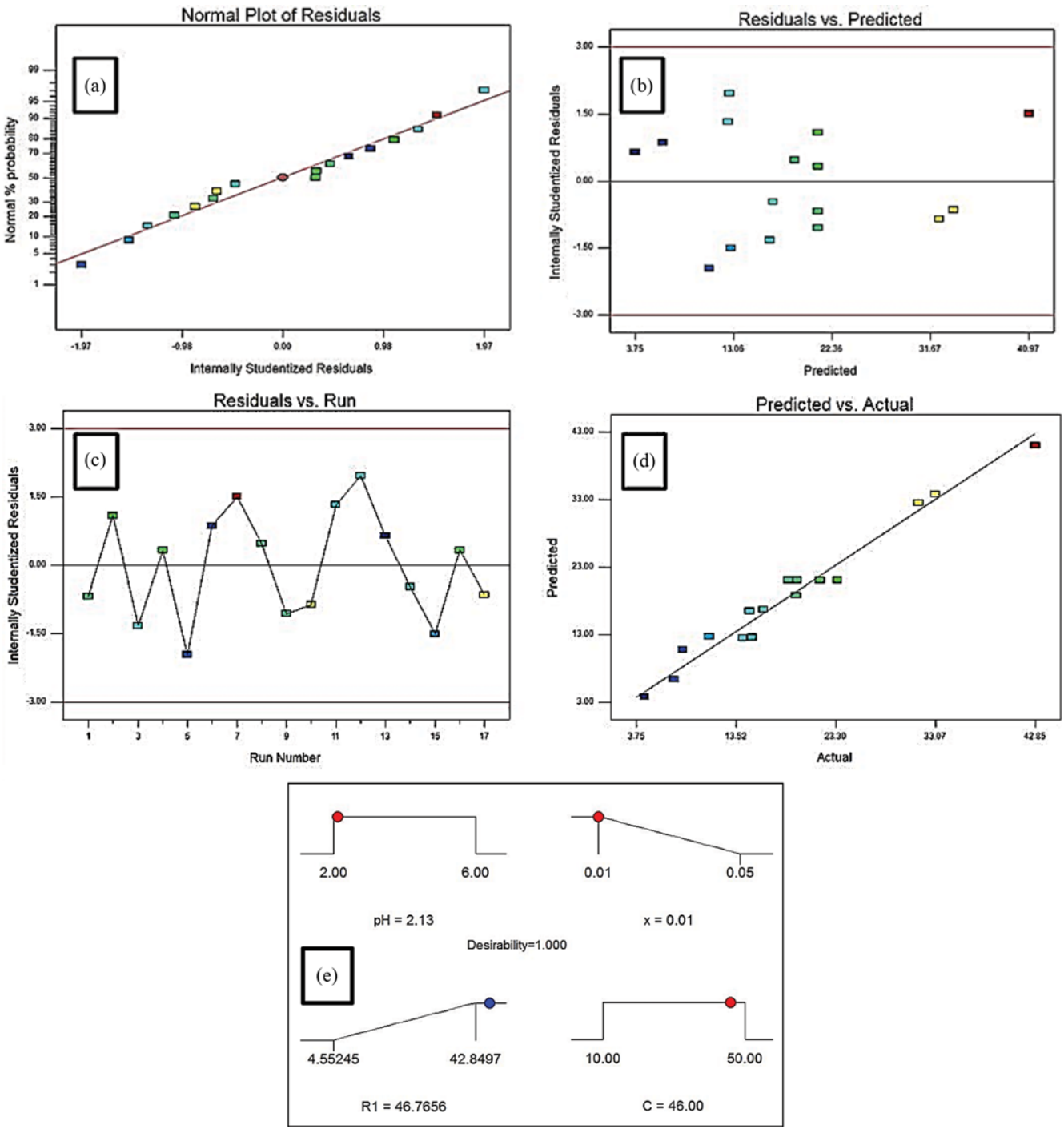

Fig. 11. (a) The studentized and the normal percentage probability plot of the removal capacity, (b) the predicted removal and the studentized residual plot, (c) the run number and the studentized residual plot, (d) the actual and the predicted removal capacity, and (e) the optimization of the response and the variables.

mined by numerical optimization [43]. Numerical optimization assigns an optimal point to each parameter through adjusting pH, adsorbent amount and initial concentration of permanganate ion to achieve maximum removal capacity. As seen in Fig. 11(e) the optimum conditions include pH=2.13, an adsorbent amount of 0.02 g, permanganate initial concentration of 46 mg/*l* which resulted in a removal capacity of 46.76 mg/g.

CONCLUSION

Natural zeolite clinoptilolite was magnetized using magnetic maghemite nanoparticles. Chitosan, which is a biodegradable and non-toxic biopolymer, was used to cover the magnetic nanocomposite and to increase its adsorption capacity. In addition, to increase the adsorption capacity, nanocomposite was functionalized

by urea that has two amine groups. Clinoptilolite/Maghemite/Chitosan/Urea nanocomposite was characterized and analyzed by XRD, VSM, SEM, and FTIR results showed that the synthesis of nanocomposite with desired structure was successful. The saturation magnetization of the final nanocomposite was 18.4 emu g^{-1}. Hence, nanocomposite was easily removed from solution by a fast and simple magnetic separation process. The effects of temperature, contact time, metal concentration, pH, and adsorbent amount on permanganate removal capacity were assessed. The kinetics of adsorption process was evaluated using pseudo-first and pseudo-second-order, Elovich and intraparticle diffusion models in which pseudo-second-order kinetic model best fitted the experimental data. Langmuir, Freundlich, Temkin and Dubinin Radushkevich isotherm models were used to study the adsorption isotherm, and the Langmuir isotherm best conformed to the data. Thermodynamic results and negative Gibbs free energy changes represent the spontaneous nature of the removal process. To achieve optimum conditions for permanganate removal, experiments were designed using response surface methodology and central composite design. The adsorption process was examined as a function of pH (4-6), the initial concentration of permanganate ions (10-50 mg/*l*) and adsorbent amount (0.01-0.05 g). Maximum removal capacity of permanganate and maximum adsorption capacity for manganese under optimal conditions of pH=2.13, an adsorbent amount of 0.02 g, permanganate initial concentration of 46 mg/*l* were 46.76 and 16.3 mg/g, respectively. Pure superparamagnetic nanocomposite showed good adsorption capacity compared to previous similar research. Thus, it can be used as an appropriate adsorbent to remove manganese from waters and wastewaters.

ACKNOWLEDGEMENT

Financial support of this work by ACECR Institute of Higher Education (Isfahan Branch) is gratefully appreciated.

SUPPORTING INFORMATION

Additional information as noted in the text. This information is available via the Internet at http://www.springer.com/chemistry/journal/11814.

REFERENCES

1. A. Abbas, A. M. Al-Amer, T. Laoui, M. J. Al-Marri, M. S. Nasser, M. Khraisheh and M. A. Atieh, *Sep. Purif. Technol.*, **157**, 141 (2016).
2. Z. Ezzeddine, I. Batonneau-Gener, Y. Pouilloux, H. Hamad, Z. Saad and V. Kazpard, *Micropor. Mesopor. Mater.*, **212**, 125 (2015).
3. A. Dąbrowski, Z. Hubicki, P. Podkościelny and E. Robens, *Chemosphere*, **56**, 91 (2004).
4. M. Sarioglu, *Sep. Purif. Technol.*, **41**, 1 (2005).
5. A. bin Jusoh, W. Cheng, W. Low, A. Nora'aini and M. M. Noor, *Desalination*, **182**, 347 (2005).
6. N. Esfandiar, B. Nasernejad and T. Ebadi, *J. Ind Eng. Chem.*, **20**, 3726 (2014).
7. A. Tekerlekopoulou and D. Vayenas, *Desalination*, **210**, 225 (2007).
8. M. Xie, L. Zeng, Q. Zhang, Y. Kang, H. Xiao, Y. Peng, X. Chen and J. Luo, *J. Alloys Compounds*, **647**, 892 (2015).
9. R. K. Gautam, S. K. Sharma, S. Mahiya and M. C. Chattopadhyaya, Contamination of heavy metals in aquatic media: Transport, toxicity and technologies for remediation (2014).
10. A. K. Meena, G. Mishra, P. Rai, C. Rajagopal and P. Nagar, *J. Hazard. Mater.*, **122**, 161 (2005).
11. M. I. Inyang, B. Gao, Y. Yao, Y. Xue, A. Zimmerman, A. Mosa, P. Pullammanappallil, Y. S. Ok and X. Cao, *Critical Reviews Environ. Sci. Technol.*, **46**, 406 (2016).
12. E. Okoniewska, J. Lach, M. Kacprzak and E. Neczaj, *Desalination*, **206**, 251 (2007).
13. P. Roccaro, C. Barone, G. Mancini and F. Vagliasindi, *Desalination*, **210**, 205 (2007).
14. E. Khoramzadeh, B. Nasernejad and R. Halladj, *J. Taiwan Institute Chem. Engineers*, **44**, 266 (2013).
15. M. Ghiaci, A. Abbaspur, R. Kia and F. Seyedeyn-Azad, *Sep. Purif. Technol.*, **40**, 217 (2004).
16. R. Hernández-Huesca, L. Díaz and G. Aguilar-Armenta, *Sep. Purif. Technol.*, **15**, 163 (1999).
17. N. Mansouri, N. Rikhtegar, H. A. Panahi, F. Atabi and B. K. Shahraki, *Environ. Protection Eng.*, **39** (2013).
18. V. Javanbakht, S. M. Ghoreishi, N. Habibi and M. Javanbakht, *Powder Technol.*, **302**, 372 (2016).
19. M. Matik, M. Václavíková and V. Šepelák, *Diffusion Fundamentals*, **12**, 86 (2010).
20. J. Hu, G. Chen and I. M. Lo, *J. Environ. Eng.*, **132**, 709 (2006).
21. S. Rajput, C. U. Pittman and D. Mohan, *J. Colloid Interface Sci.*, **468**, 334 (2016).
22. A. H. Lu, E. e. L. Salabas and F. Schüth, *Angewandte Chemie International Ed.*, **46**, 1222 (2007).
23. P. L. Hariani, M. Faizal and D. Setiabudidaya, *Int. J. Environ. Sci. Development*, **4**, 336 (2013).
24. M. V. Dinu and E. S. Dragan, *Chem. Eng. J.*, **160**, 157 (2010).
25. E. Darezereshki, *Mater. Lett.*, **64**, 1471 (2010).
26. E. Darezereshki, M. Ranjbar and F. Bakhtiari, *J. Alloys Compounds*, **502**, 257 (2010).
27. H. Jahangirian, M. Shah Ismail, M. J. Haron, R. Rafiee-Moghaddam, K. Shameli, S. Hosseini, K. Kalantari, R. Khandanlou, E. Gharibshahi and S. Soltaninejad, *Dig. J. Nanomaterials Bios*, **4**, 4 (2013).
28. H. Faghihian, M. Moayed, A. Firooz and M. Iravani, *Comptes Rendus Chimie*, **17**, 108 (2014).
29. K. Petcharoen and A. Sirivat, *Mater. Sci. Eng.: B*, **177**, 421 (2012).
30. R. G. López, M. G. Pineda, G. Hurtado, R. D. d. León, S. Fernández, H. Saade and D. Bueno, *Int. J. Mole. Sci.*, **14**, 19636 (2013).
31. G. Unsoy, S. Yalcin, R. Khodadust, G. Gunduz and U. Gunduz, *J. Nanoparticle Res.*, **14**, 964 (2012).
32. Y. Tan, M. Chen and Y. Hao, *Chem. Eng. J.*, **191**, 104 (2012).
33. K. Foo and B. Hameed, *Chem. Eng. J.*, **156**, 2 (2010).
34. G. Zhao, X. Wu, X. Tan and X. Wang, *Open Colloid Sci. J.*, **4** (2010).
35. G. Bayramoğlu and M. Y. Arica, *Chem. Eng. J.*, **139**, 20 (2008).
36. Y.-M. Hao, C. Man and Z.-B. Hu, *J. Hazard. Mater.*, **184**, 392 (2010).
37. X. Huang, N.-y. Gao and O.-l. Zhang, *J. Environ. Sci.*, **19**, 1287 (2007).
38. M. Al-Ghouti, M. Khraisheh, M. Ahmad and S. Allen, *J. Colloid Interface Sci.*, **287**, 6 (2005).

39. N. Yahaya, M. Pakir, M. Latiff, I. Abustan, O. Bello and M. Ahmad, *Int. J. Eng. Technol.*, **10**, 132 (2010).
40. V. Javanbakht and S. M. Ghoreishi, *Ads. Sci. Technol.*, **35**, 241 (2017).
41. V. Javanbakht, H. Zilouei and K. Karimi, *Int. Biodeterioration Biodegradation*, **65**, 294 (2011).
42. W. W. Ngah, L. Teong and M. Hanafiah, *Carbohydrate Polym.*, **83**, 1446 (2011).
43. A. Ahmadi, S. Heidarzadeh, A. R. Mokhtari, E. Darezereshki and H. A. Harouni, *J. Geochem. Exploration*, **147**, 151 (2014).

Supporting Information

Preparation and characterization of a novel nanocomposite of clinoptilolite/maghemite/chitosan/urea for manganese removal from aqueous solution

Zahra Sareban and Vahid Javanbakht[†]

ACECR Institute of Higher Education (Isfahan Branch), Isfahan, 84175-443, Iran
(*Received 15 May 2017 • accepted 4 August 2017*)

Table S1. The spectra points of FTIR analysis are shown in the table as supplementary file

Clinoptilolite		Maghemite		Chitosan	
Peak (cm^{-1})	Bond	Peak (cm^{-1})	Bond	Peak (cm^{-1})	Bond
3420	O-H stretching bond	3396	Stretching mode of H_2O molecules or hydroxyl groups on the surface	3432	Stretching vibrations of O-H, extensive vibrations of N-H
1641	O-H bending vibrations	1617	Bending vibrations of H_2O	2923	C-H stretching vibrations
797	Stretching and bending bonds of Si-O and Al-O	579	Stretching vibrations of Fe-O bond	1634	Stretching vibrations of NHCO, bending bonds of N-H and NH_2
1090	Stretching bonds inside the tetrahedron	424	Octagonal stretching bond of iron	1417	Stretching vibration of C-N
				1383	Bending vibration of CH_3
				1085	Stretching vibration of C-OH